

**Energy-storage performance of NaNbO₃ based multilayer capacitors**

Journal:	<i>Journal of Materials Chemistry C</i>
Manuscript ID	TC-ART-04-2021-001826.R1
Article Type:	Paper
Date Submitted by the Author:	18-May-2021
Complete List of Authors:	Zhu, Lifeng; University of Science and Technology Beijing, Yan, Yongke; Penn State University Park Leng, Haoyang; The Pennsylvania State University Department of Materials Science and Engineering Li, Xiaotian; The Pennsylvania State University Department of Materials Science and Engineering Cheng, Li-Qian; The Pennsylvania State University - University Park Campus Priya, Shashank; Pennsylvania State University

Energy-storage performance of NaNbO_3 based multilayer capacitors

Li-Feng Zhu^{1,2,3}, Yongke Yan^{*2}, Haoyang Leng², Xiaotian Li², Li-Qian Cheng², Shashank Priya^{*2}

¹ School of Materials Science and Engineering, University of Science and Technology Beijing, Beijing 100083, China.

² Department of Materials Science and Engineering, The Pennsylvania State University, University Park, PA 16802, United States

³ Foshan (Southern China) Institute for New Materials, Foshan, Guangdong, 528200, China.

Abstract

Environmentally friendly NaNbO_3 capacitors have a great potential for applications in pulsed-discharge and power conditioning electronic systems because of their AFE-like hysteresis behavior, high saturation polarization and low mass. Here we demonstrate $(0.96-x)\text{NaNbO}_3-0.04\text{CaZrO}_3-x\text{Bi}_{0.5}\text{Na}_{0.5}\text{TiO}_3$ (abbreviated as NN-CZ- x BNT) capacitors with high energy storage density (W_{rec}) and efficiency (η). The performances of capacitors were tuned by the composition induced relaxor behavior and grain refinement which resulted in reduction of the hysteresis and increase in the breakdown strength (BDS). Two-step sintering is found to be effective for reducing the grain size of MLCCs to 3 μm , which is 86% smaller as compared to grain size obtained by conventional solid-state sintering (22 μm). Small grain size significantly reduces the leakage current and losses and increases the BDS, yielding excellent $W_{\text{rec}} = 3.7 \text{ J/cm}^3$ and $\eta = 82.1\%$ in the NN-0.04CZ-0.16BNT multilayer capacitors. Results provide a systematic strategy for enhancing the energy storage density and efficiency of dielectric capacitors through the combination of dielectric relaxation and grain size refinement.

Keywords: Dielectrics; Multilayer; Ceramic; Capacitors; Grain size; NaNbO_3 ; Energy storage

Corresponding author: yxy355@psu.edu (Yongke Yan)

Corresponding author: sup103@psu.edu (Shashank Priya)

Introduction

Dielectric capacitors provide several key advantages, such as high power-density, fast charge/discharge rate, fatigue resistance and high temperature stability. This makes them possessed promising for applications in pulsed-discharge and power conditioning electronic systems, such as hybrid electric vehicles, high-powered accelerators, space shuttle power systems, and kinetic energy weapons [1-6]. However, the energy-storage density (W) of dielectric capacitors is extremely low in comparison with that of batteries or electrochemical capacitors. Theoretically, the W of the dielectric capacitor can be calculated by numerical integration of the electric-field-polarization (P-E) loops between the maximum polarization and the origin, based on the following equations [7,8]:

$$W = \int_0^{D_{\max}} E dD \approx \int_0^{P_{\max}} E dP \quad (1)$$

$$W_{re} \approx \int_{P_r}^{P_{\max}} E dP \quad (2)$$

$$\eta = \frac{W_{re}}{W} \times 100\% \quad (3)$$

where E , D and D_{\max} are the electric field, electric displacement, and maximum electric displacement under the applied electric field; P , P_r and P_{\max} represent the polarization, remanent polarization, and the maximum polarization; and W , W_{rec} and η represent the total energy storage density, recoverable energy storage density and energy storage efficiency, respectively.

Simultaneous achievement of a small P_r , high P_{\max} and high breakdown field (BDS) are extremely important for improving the W_{rec} and η of capacitors [9]. Among different choices of antiferroelectric (AFE) ceramics [10-12], relaxor ferroelectric (RFE) ceramics [13, 14], normal ferroelectric (FE) [15] and linear nonpolar dielectric materials [16]. AFE and RFE ceramics are promising for energy storage application. AFE dielectric capacitors exhibit double P - E hysteresis loop as a result of electric-field-induced reversible AFE-FE phase transition. This is beneficial for achieving high W_{rec} value, because these materials possess high P_{\max} and extremely low P_r . For example, W_{rec} of 3~11 J/cm³ has been reported in PbZrO₃-based AFE ceramics [10,11,17-19]. However, considering the adverse effect of lead oxide on the environment and

human health, it is important to focus future investigations on lead-free ceramics [20-22].

NaNbO₃-based ceramics are attractive lead-free AFE dielectric capacitors due to presence of AFE-like hysteresis loops and high saturation polarization. For example, an ultrahigh $P_{\max} \sim 60 \mu\text{C}/\text{cm}^2$ has been obtained in 0.76NaNbO₃-0.24(Bi_{0.5}Na_{0.5})TiO₃ relaxor AFE ceramic [23]. Further, low-theoretical-density ($\rho = 4.494 \text{ g}/\text{cm}^3$) makes NaNbO₃-based capacitors makes them attractive for applications in the light-weight devices. However, limited number of studies have been conducted on energy storage applications for pure NaNbO₃ ceramics. One of the main reasons is that it has been difficult to obtain double P-E hysteresis loops at room temperature due to the small difference in free energy between its metastable FE phase (P21ma) and AFE phase (Pbma). Thus, the electric field induced FE phase is preserved after the electric field is removed, which results in a ferroelectric P-E hysteresis loop [24-31]. There have been several attempts towards stabilizing the antiferroelectric phase and exploiting its potential for antiferroelectric energy storage devices [32-34]. For example, Shimizu et al. [32] reported that the antiferroelectricity of NaNbO₃-based ceramics can be stabilized by lowering the tolerance factor, through Zr⁴⁺ and Ca²⁺ substitutions for Nb⁵⁺ and Na⁺ ion simultaneously. A moderate $W_{\text{rec}} \sim 0.55 \text{ J}/\text{cm}^3$ was obtained in the (1-x)NaNbO₃-xCaZrO₃ ceramics at x=0.04 where AFE phase can be partially stabilized (AFE and FE phase coexistence) [33]. A stable AFE orthorhombic phase has been reported in (0.94-x)NaNbO₃-0.06BaZrO₃-xCaZrO₃ ceramics at $0.01 < x \leq 0.05$, which exhibits an excellent $W_{\text{rec}} \sim 1.59 \text{ J}/\text{cm}^3$ at x=0.04, but its η was just 30% [34].

It is well-known that AFE capacitors usually exhibit a typical double P-E hysteresis loops, along with low η because of the large hysteresis between AFE-FE and FE-AFE [35,36], which results in a large portion of the charged electric energy being dissipated as heat during discharging. Further, temperature rise resulting due to large hysteresis relates loss drastically decreases the breakdown strength (BDS) of capacitors. All these issues have limited the advancement of NaNbO₃-based capacitors. A slim hysteresis loop can be obtained by tailoring the composition to realize relaxor AFE structure. For example, Li et al. [12] indicated that (Na_{0.5}Bi_{0.5})TiO₃-x(Sr_{0.7}Bi_{0.2})TiO₃ relaxor AFE capacitor was achieved by introducing (Sr_{0.7}Bi_{0.2})TiO₃ to

form a solid solution with $(\text{Na}_{0.5}\text{Bi}_{0.5})\text{TiO}_3$, which exhibited ultrahigh $\eta = 92\%$ and $W_{\text{rec}} = 9.5 \text{ J/cm}^3$. Thus, it can be expected that W_{rec} and η are enhanced by incorporating the relaxor behavior in NaNbO_3 -based ceramics.

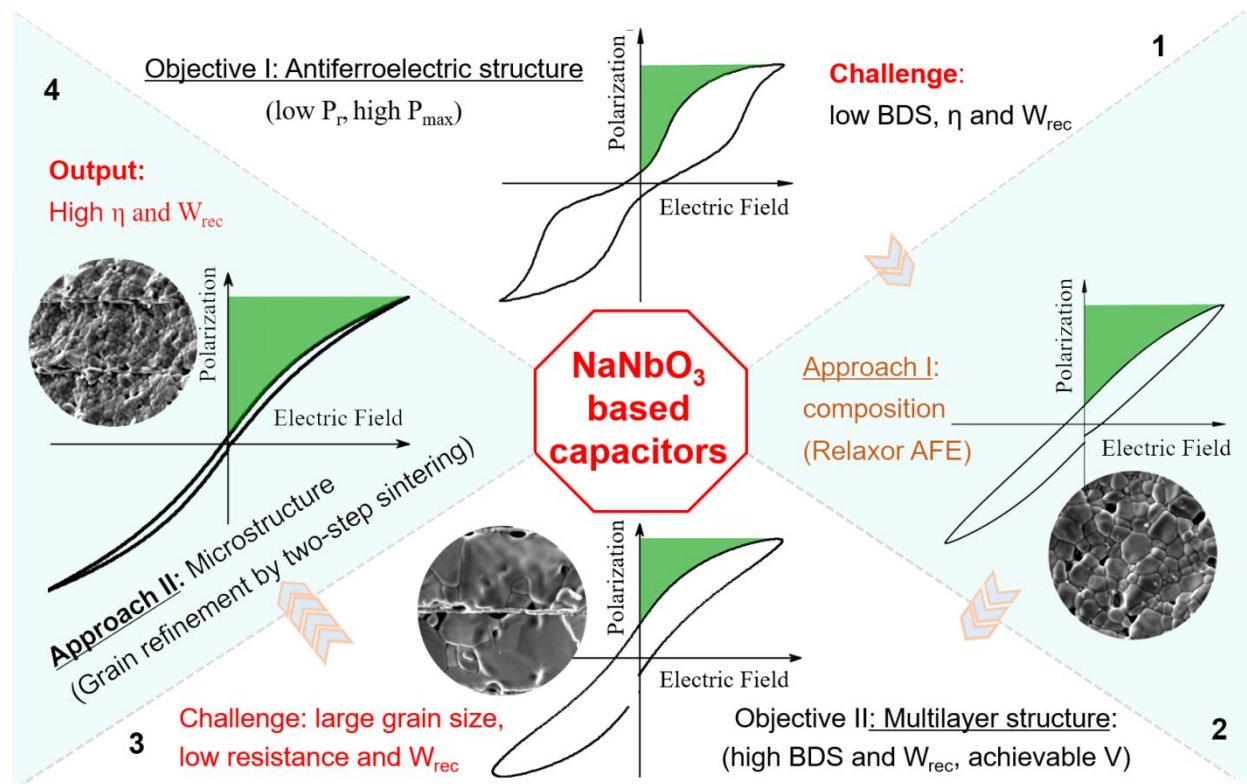


Fig. 1. Schematic diagram describing the strategies adopted for improving the W_{rec} and η of NaNbO_3 based capacitors through the combination of composition optimization and grain refinement.

Our prime objective in this study was to synthesize relaxor NaNbO_3 -based capacitors which can provide both excellent W_{rec} and η . As illustrated in Figure 1, we selected NaNbO_3 - CaZrO_3 system as the base composition, which has stable antiferroelectric phase structure. The base system, NaNbO_3 - γCaZrO_3 , was modified with $\text{Bi}_{0.5}\text{Na}_{0.5}\text{TiO}_3$ composition to form a solid solution and impart relaxor AFE behavior. Multilayer structure was designed to reduce the maximum voltage required for saturation and thereby, further increase the W_{rec} and BDS. Lastly, grain refinement via two-step sintering was achieved that led to reduction in the leakage current and increase in the reliability of thin active dielectric layer. Based on these strategies, excellent $W_{\text{rec}}=3.7 \text{ J/cm}^3$ and $\eta=82.1\%$ were achieved in NaNbO_3 - γCaZrO_3 - $x\text{Bi}_{0.5}\text{Na}_{0.5}\text{TiO}_3$ MLCCS. Combined all these strategies, provide an effective approach for designing and manufacturing

capacitors with high W_{rec} and high η .

Experimental

Sodium carbonate (Na_2CO_3 , 99.0%), niobium pentoxide (Nb_2O_5 , 99.9%), calcium carbonate (CaCO_3 , 99%), zirconium dioxide (ZrO_2 , 99%), bismuth oxide (Bi_2O_3 , 99.0%) and titanium dioxide (TiO_2 , 99.0%) were used as raw materials. These powders were weighed according to the compositions of $(0.96-x)\text{NaNbO}_3-0.04\text{CaZrO}_3-x\text{Bi}_{0.5}\text{Na}_{0.5}\text{TiO}_3$ (abbreviated as NN-CZ- x BNT, $x=0.12, 0.14, 0.16$ and 0.18) and mixed with alcohol. After drying the slurry and calcining at $900\text{ }^\circ\text{C}$ for 5 h in an air atmosphere, the resultant powders were remixed and pressed into disks of 12 mm in diameter and 1.0 mm in thickness without any binders. The pellets were further pressed using cold isostatic pressing (CIP: Autoclave Engineers, Flow Autoclave Systems, Inc.), and then sintered at $1200\text{ }^\circ\text{C}$ - $1280\text{ }^\circ\text{C}$ for 2 h in an air atmosphere. To reduce the applied voltage into the range of power supply, the sintered bulk ceramics was grinded to $170\text{ }\mu\text{m}$ in thickness. These bulk ceramic samples were coated with silver paste on the upper and bottom surfaces and fired at $550\text{ }^\circ\text{C}$ for 30 min for the electrical measurement.

The MLCCs samples were prepared by the tape-casting method. To obtain a fine slurry, the milled $0.80\text{NN}-0.04\text{CZ}-0.16\text{BNT}$ powders (56 wt%) were added into a solution of Xylene (17 wt%), ethanol (17 wt%), menhaden fish oil (1.2 wt%), polyethylene glyco 400 (1.5 wt%), butyl benzyl phthalate (1.5 wt%) and Polyvinyl Butyral (PVB, 3wt%) mixture and ball-milled for 24 h. Tape casting was performed on a laboratory-type tape-casting machine using a doctor blade with $100\text{ }\mu\text{m}$ opening. The green tapes were cut into square samples of 1-inch in length. Layers of $0.80\text{NN}-0.04\text{CZ}-0.16\text{BNT}$ green tapes were stacked and laminated using a uniaxial hot press at $60\text{ }^\circ\text{C}$ to achieve a single thick dielectric layer. Pt paste was screen-printed as internal electrode on top of the dielectric layer. Screen-printed layers were stacked and laminated to form MLCCs. The multilayer capacitors were sintered by conventional solid-state sintering (CSS) and two-step sintering methods, respectively, as shown in Fig.2.

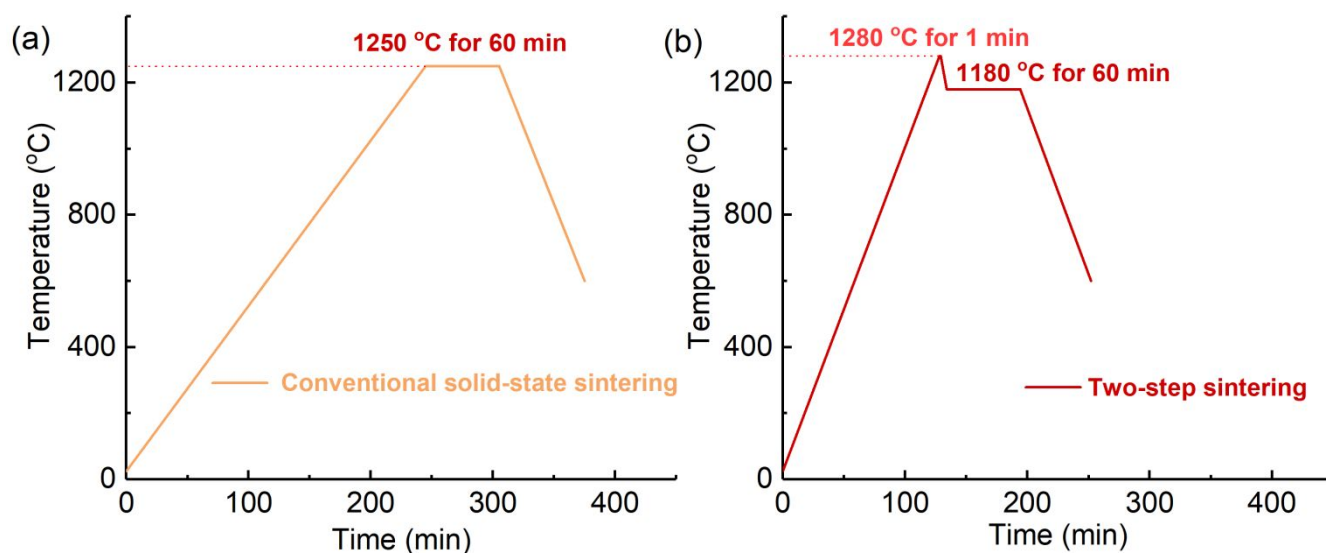


Fig. 2. Sintering process for multilayer capacitors (a) conventional solid-state sintering (sintering at 1250 °C for 60 min) and (b) two-step sintering (first sintering at 1280 °C for 1 min, and then fast cooling to 1180 °C and dwelling 60 min).

The crystal structure was studied by using XRD with a Cu $K\alpha$ radiation ($\lambda=1.5406 \text{ \AA}$) filtered through a Ni foil (XRD, Panalytical Empyrean). Ferroelectric hysteresis loops were measured by precision 10 kV HVI-SC precision materials analyzer (Radiant technologies INC, USA). The microstructure of the multilayer capacitors was evaluated using field-emission scanning electron microscopy (FESEM Apreo, Thermo Fisher) in combination with energy dispersive spectroscopy (EDS), and their average grain sizes were measured by the Nano Measurer 1.2 software from SEM images. The temperature dependence of dielectric properties was examined using a programmable furnace with an E4980AL Precision LCR Meter at 1 kHz in a temperature range of -140 °C to 80 °C.

3. Results and discussion

Figure 3 presents the temperature dependence of dielectric properties (dielectric constant ϵ_r and dielectric loss $\tan \delta$) at different frequencies from 1 kHz to 20 kHz for NN-0.04CZ- x BNT ceramics in the range of $0.12 \leq x \leq 0.18$. All samples show a very broad dielectric peak around T_m (dielectric maximum temperature) and the T_m shifts remarkably to higher temperature with increasing frequency, suggesting relaxor ferroelectric like behavior [37-39]. To further verify the relaxor behavior, the Curie-Weiss law [40],

as shown in equation (1), was employed to calculate the diffuseness degree (γ), which varies from 1 (normal ferroelectric) to 2 (typical relaxor ferroelectric) [41]. For NN-0.04CZ- x BNT ceramics, the γ value lies in between 1.514 and 1.629, indicating typical relaxor-characteristics, and γ value increases with increasing x , which suggests that relaxor behavior of NN-0.04CZ- x BNT ceramics becomes more obvious.

$$\frac{1}{\varepsilon_r} - \frac{1}{\varepsilon_m} = \frac{(T - T_m)^r}{C'} \quad (1)$$

where C' is the Curie-like constant, and T_m is the temperature corresponding to ε_m .

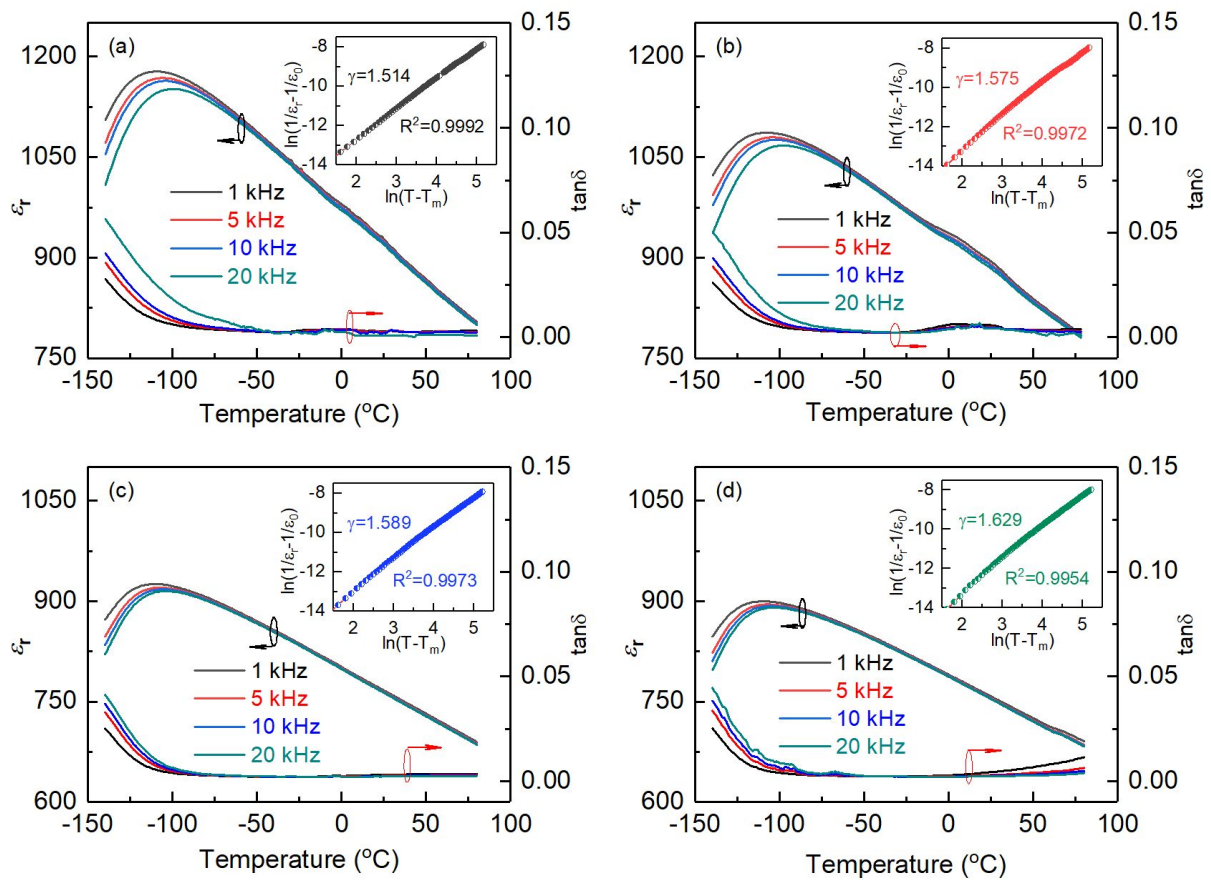


Fig. 3. Temperature dependence of the dielectric permittivity and loss measured at different frequencies from 1 kHz to 20 kHz for NN-0.04CZ- x BNT ceramics with $0.12 \leq x \leq 0.18$. The insets show the plots of $\ln(1/\varepsilon_r - 1/\varepsilon_m)$ versus $\ln(T - T_m)$ at 20 kHz for the corresponding ceramics, $x=0.12$ (a), $x=0.14$ (b), $x=0.16$ (c) and $x=0.18$ (d)

Figure 4a presents the unipolar P-E loops of NN-0.04CZ- x BNT ceramics with $0.12 \leq x \leq 0.18$. As the value of x increases, the P-E loops become slim along with decrease of P_{\max} and P_r , which indicates

strengthening of relaxor behavior and the appearance of polar nano regions. The variation of ΔP , that is the difference between P_{\max} and P_r ($\Delta P = P_{\max} - P_r$), for NN-0.04CZ- x BNT ceramics measured at different electric field (E_f) is shown in Fig.4b. Under same electric field condition, the ΔP value decreases with increasing x , which is undesirable for the improvement of W_{rec} . However, with increasing x , the BDS of NN-0.04CZ- x BNT ceramics first increases and then decreases. The maximum BDS of 350 kV/cm was achieved in the ceramics with $x=0.16$. Because of high BDS and a relatively large ΔP , an excellent $W_{\text{rec}} = 3.2 \text{ J/cm}^3$ was achieved in the ceramics with $x=0.16$ as shown in Fig.4c. Moreover, an excellent efficiency $\eta > 87\%$ was obtained in the ceramics with $x=0.16$ as shown in Fig. 4d, due to the presence of slim P-E loop as shown in Fig.3a and FigS3. Excellent value of $W_{\text{rec}} = 3.2 \text{ J/cm}^3$ and $\eta > 87\%$ are achieved in the ceramics with $x=0.16$ demonstrating that $\text{Bi}_{0.5}\text{Na}_{0.5}\text{TiO}_3$ induced relaxor behavior is an effective approach for improving BDS, W_{rec} and η of AFE NaNbO_3 ceramics.

Reliable temperature stability is one of the key factors for ensuring the operation of energy storage devices in a wide temperature range. Thus, the temperature dependence of P-E loops and energy storage capability of 0.80NN-0.04CZ-0.16BNT ceramics are investigated as displayed in Fig. 5a and b, in which the electric field and frequency were fixed at 250 kV/cm and 10 Hz, respectively. There is almost no change in P_{\max} with increasing the temperature, while the P_r slightly rises when the temperature increases as shown in Fig. 5a and Fig S5a, indicating the small deterioration of the W_{rec} . Overall, the amplitude of fluctuations in W_{rec} is less 15% in the temperature range between 24 °C and 120 °C as displayed in Fig. 5b. The frequency dependence of the unipolar P-E loops and W_{rec} of 0.80NN-0.04CZ-0.16BNT ceramics are shown in Fig. 5c and d. It can be observed that P_{\max} and P_r slightly decreases with increase in frequency. Nonetheless, the W_{rec} remains stable when the frequency increases, and the fluctuations in W_{rec} is less than 5% as shown in Fig. 5c. Hence, it can be concluded that the 0.80NN-0.04CZ-0.16BNT ceramics possess a good frequency and temperature stability, that meets the capacitor requirements.

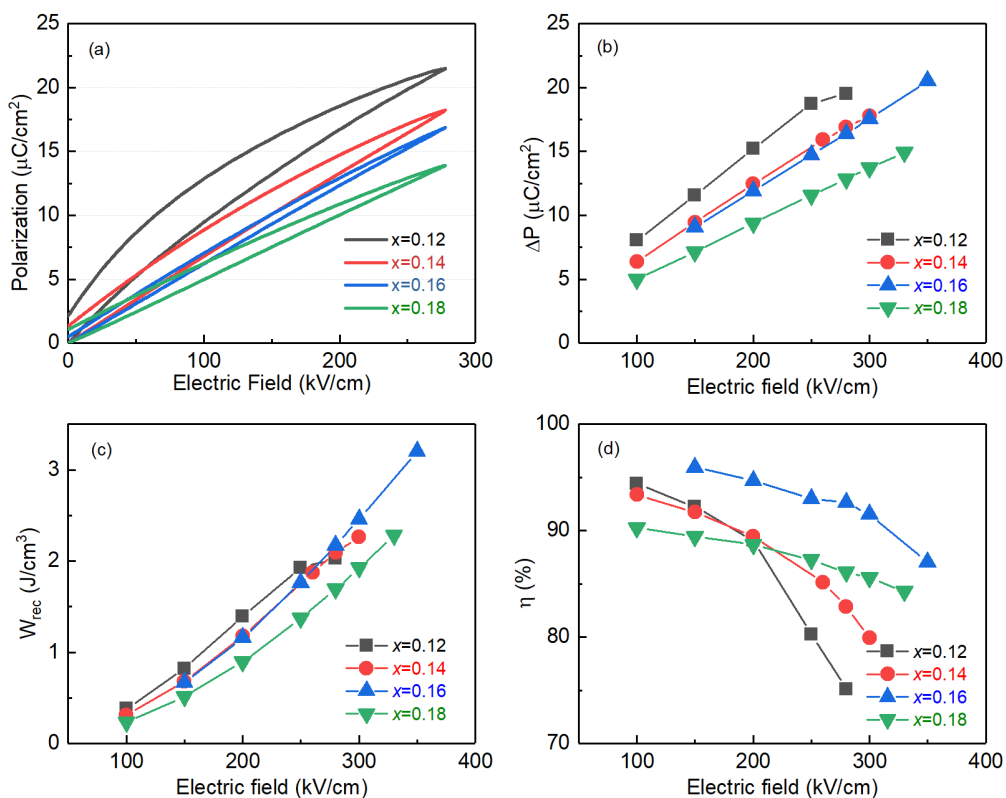


Fig. 4 Unipolar P-E hysteresis loops (a), ΔP value (b), Recoverable energy storage density W_{rec} (c) and energy storage efficiency η (%) (d) for $(0.96-x)\text{NN}-0.04\text{CZ}-xB\text{NT}$ ceramics at $0.12 \leq x \leq 0.18$.

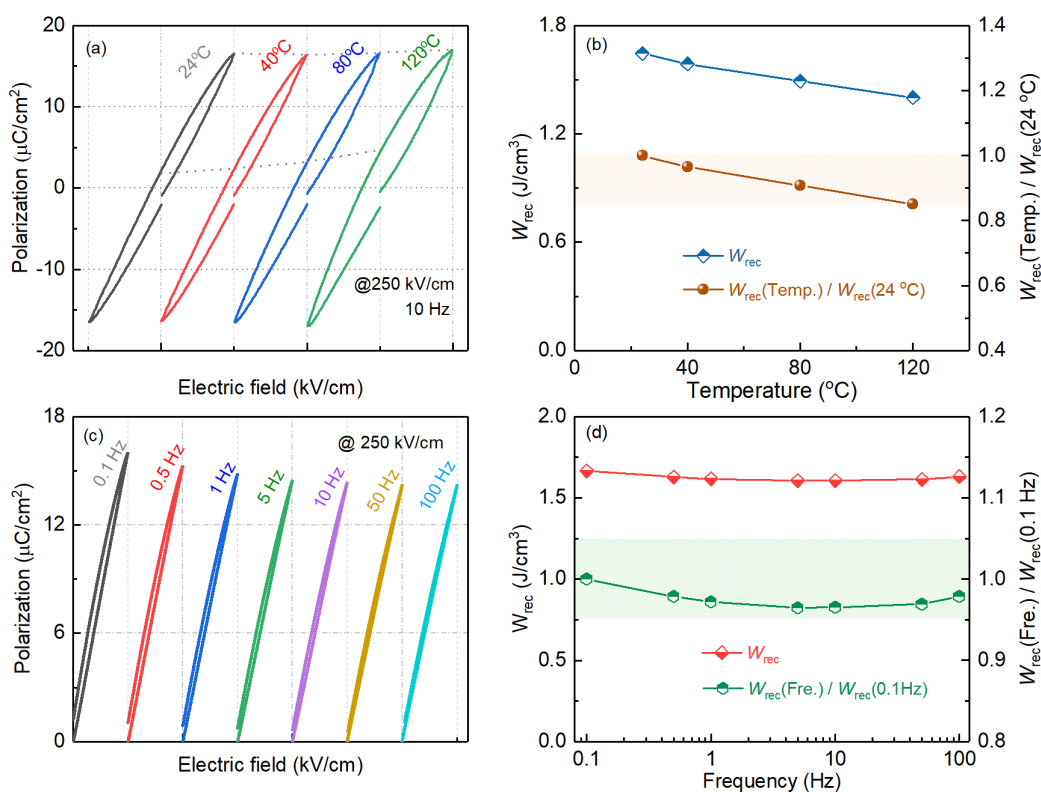


Fig. 5. Bipolar P-E hysteresis loops measured at different temperature (24~120 °C) (a), W_{rec} versus temperature (b), unipolar P-E hysteresis loops measured at different frequencies (0.1~100 Hz) (c) and W_{rec} versus frequencies (d) for 0.80 NN-0.04CZ-0.16BNT ceramics, respectively.

To further enhance the energy-storage density of the NN-0.04CZ-*x*BNT ceramic, multilayer capacitors (MLCCs) were fabricated via the tape casting method, as shown in Figure 6a. The thicknesses of single ceramic layer and Pt electrodes are 29 and 2 μm , respectively (Figure 6b). All elements in each layer are uniformly distributed (Fig. 6c). Based on the microstructure shown in Fig. 6b, it can be observed that there are only one or two grains along the thickness direction due to the large grain size, which significantly reduces the BDS and reliability of NN-0.04CZ-0.16BNT MLCCs. Yang [42] has pointed out that the BDS has an exponential decay relationship with the grain size, i.e., $\text{BDS} \propto (\text{grain size})^{-a}$ with exponent values being in the range of 0.2-0.4 ($a = 0.2-0.4$). To improve the BDS, a two-step sintering (TSS) method was adopted. TSS has been widely used method for decreasing the grain size of ceramics [43,44]. As shown in Fig. 7, it can be observed that the grain size in MLCCs can be reduced from 22 μm , sintered by the conventional solid-state sintering (CSS) method, to about 3 μm sintered by using the TSS method, which is even lower than 7 μm obtained in bulk ceramics.

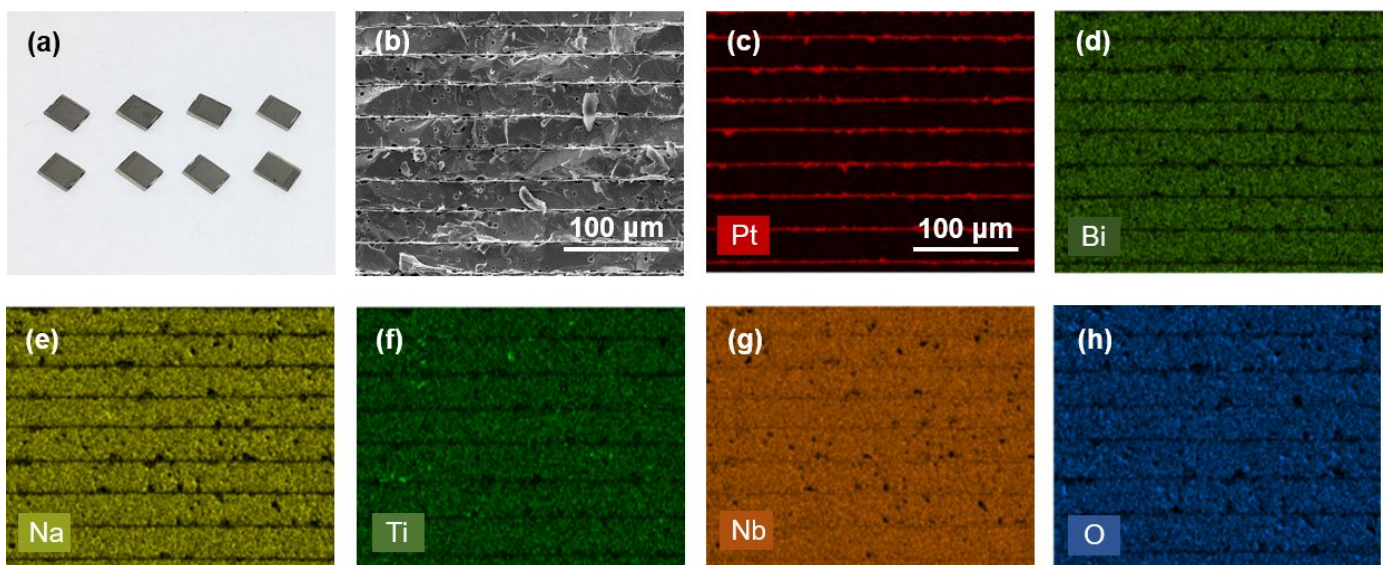


Fig 6 Picture and microstructures of multilayer ceramic 0.80NN-0.04CZ-0.16BNT. (a) Pictures of the synthesized NN-0.04CZ-0.16BNT MLCCs. (b) SEM images of the MLCCs, showing the ceramic and electrode layers. (c), (d), (e), (f), (g), (h) SEM/EDX images on the distributions of specific elements (Pt, Bi, Na, Ti, Nb, and O).

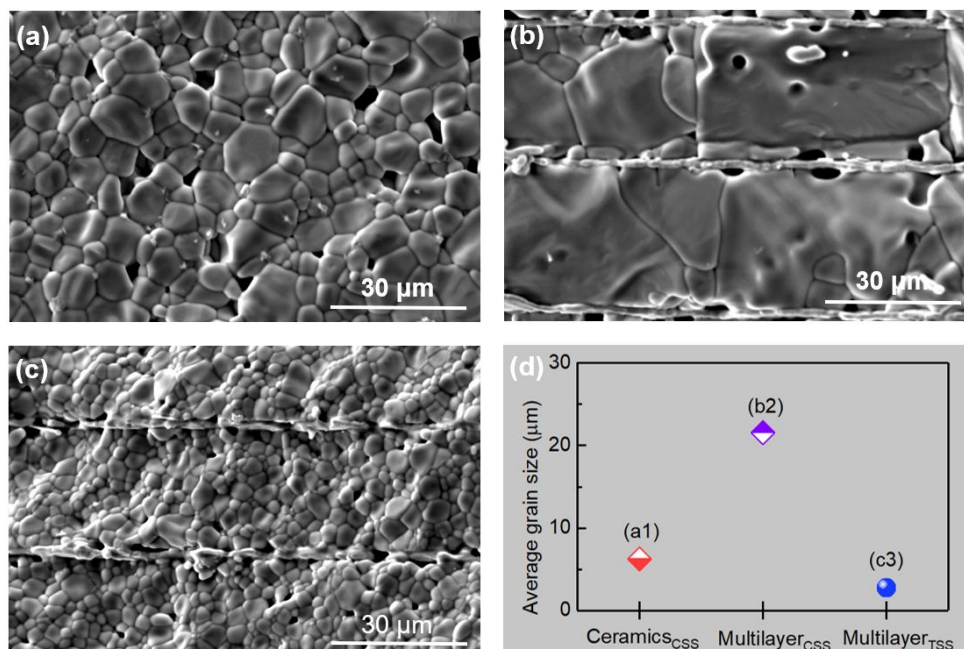


Fig.7 SEM images of fractured surface for: (a) 0.80NN-0.04CZ-0.16BNT bulk ceramics (Ceramic_{CSS}), (b) multilayer capacitors sintered by conventional solid-state sintering at sintering temperature of 1250 °C for 60min (Multilayer_{CSS}) and (c) sintered by two-step sintering, first 1280 °C for 1min, then 1180 °C for 60min (Multilayer_{TSS}), and (d) average grain size obtained through different processing techniques.

Figure 8 presents the energy storage performance of NN-0.04CZ-0.16BNT MLCCs. The MLCCs sintered by CSS method possess large grains and lossy P-E loops as shown in Fig 8a and 8b, and thus the W_{rec} and η calculated from P-E loops, as shown in Fig.8c, are only 1.8 J/cm³ and 43.4%, respectively, far lower than the values of 3.2 J/cm³ and 87.1% obtained for NN-0.04CZ-0.16BNT ceramics, as shown in Fig.4. This is due to the large grain size in NN-0.04CZ-0.16BNT MLCCs, which leads to the increase of leakage current, making the P-E loops lossy and decreasing the BDS [42]. Comparing with MLCCs sintered by CSS, the samples sintered by TSS method possess small grain, low porosity and slim P-E loops as shown in Fig 8d and 8e and an excellent W_{rec} =3.7 J/cm³ and η =82.1% measured at 400 kV/cm as shown in Fig 8f. The improvement of W_{rec} and η for NN-0.04CZ-0.16BNT MLCCs sintered by TSS method can be attributed to the following reasons: (i) Fine-grain capacitors possess high grain boundary density which provides depletion regions [42] that assist in the improvement of leakage current and BDS of MLCCs. (ii) low sintering temperature of 1180 °C using the TSS technology is beneficial for reducing the volatilization of sodium ions, defect concentration and porosity in comparison to high temperature of 1250 °C for CSS

method, resulting in the enhancement of resistance and BDS. Based on these results, it is clear that TSS method is useful for increasing the BDS and energy storage of MLCCs.

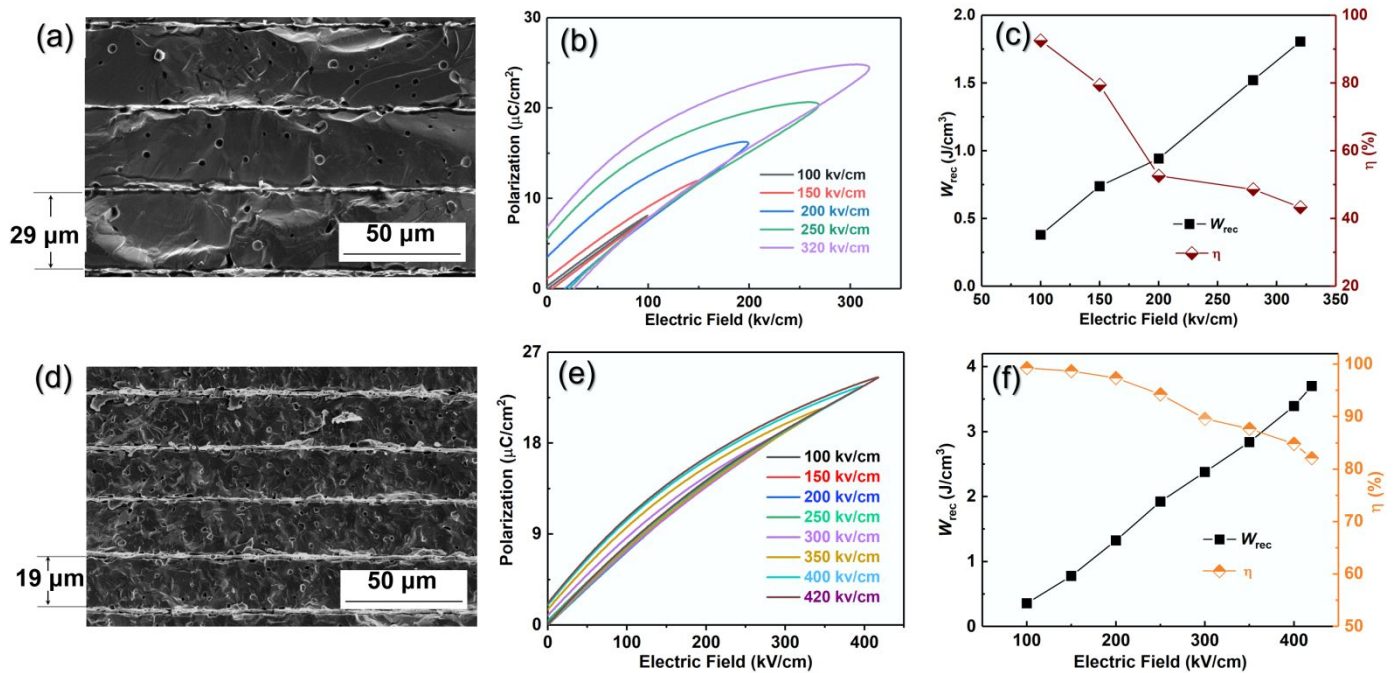


Fig. 8. Microstructure and energy-storage performance of 0.80NN-0.04CZ-0.16BNT multilayer capacitors using different sintering processes, SEM images of capacitors (a) and (d), Unipolar P-E hysteresis loops (b) and (e), and energy storage density W_{rec} and energy storage efficiency η (%) (c) and (f).

Conclusions

Environment-friendly NaNbO_3 AFE system has received extensive attention as an energy-storage material because of its high saturation polarization and W_{rec} , but its application has been limited by high degree of polarization hysteresis. Here, we adopted a combination of the composition induced relaxor ferroelectric behavior and microstructural grain refinement to reduce the hysteresis and improve the BDS. The relaxor behavior was introduced by adding BNT relaxor end component, while the grain refinement was achieved by employing a two-step sintering process. With this method, an excellent $W_{\text{rec}} = 3.7 \text{ J/cm}^3$ and $\eta = 82.1\%$ are achieved in the NN-0.04CZ-0.16BNT multilayer capacitors.

Acknowledgments

L.F. from China was supported by China Scholarship council (Grant No. 2019064665016), Guangdong

Basic and Applied Basic Research Foundation (Grant No. 2019A1515110688), and acknowledge the support through National Natural Science Foundation of China (Grant No. 52032007). Y.Y. and X.L. acknowledge the support through National Science Foundation through the award number DMR-1936432. H.L. acknowledges the support through DARPA program HR00111920001. S.P. acknowledges the support through National Science Foundation international program (OISE-1829573).

References

- [1] C.A. Randall, H. Ogihara, J.R. Kim, G.Y. Yang, C.S. Stringer, S. Trolier-McKinstry, M. Lanagan, High temperature and high energy density dielectric materials. In Proceedings of the Pulsed Power Conference, Washington, DC, USA, 2009; 346–351.
- [2] Prateek, V.K. Thakur, R.K. Gupta, Recent progress on ferroelectric polymer-based nanocomposites for high energy density capacitors: synthesis, dielectric properties, and future aspects, *Chem. Rev.*, 2016, 116(7):4260-4317.
- [3] Q. Li, F.Z. Yao, Y. Liu, G. Zhang, H. Wang, Q. Wang, High-temperature dielectric materials for electrical energy storage, *Annu. Rev. Mater. Res.*, 2018, 48:219-243.
- [4] Z. Yao, Z. Song, H. Hao, Z. Yu, M. Cao, S. Zhang, M. T. Lanagan, H. Liu, Homogeneous/inhomogeneous-structured dielectrics and their energy-storage performances, *Adv. Mater.*, 2017, 29(20):1601727.
- [5] H. Palneedi, M. Peddigari, G.T. Hwang, D.Y. Jeong, J. Ryu, High-performance dielectric ceramic films for energy storage capacitors: progress and outlook, *Adv. Funct. Mater.*, 2018, 28:1803665.
- [6] F.Z. Yao, Q. Yuan, Q. Wang, H. Wang, Multiscale structural engineering of dielectric ceramics for energy storage applications: from bulk to thin films, *Nanoscale*, 2020, 12:17165-17184

- [7] B. Peng, Q. Zhang, X. Li, T. Sun, H. Fan, S. Ke, M. Ye, Y. Wang, W. Lu, H. Niu, J. F. Scott, X. Zeng, H. Huang, Giant electric energy density in epitaxial lead-free thin films with coexistence of ferroelectrics and antiferroelectrics, *Adv. Electron. Mater.*, 2015, 1(5):1500052.
- [8] B. Li, Q.X. Liu, X.G. Tang, T.F. Zhang, Y.P. Jiang, W.H. Li, J. Luo, Antiferroelectric to relaxor ferroelectric phase transition in PbO modified $(\text{Pb}_{0.97}\text{La}_{0.02})(\text{Zr}_{0.95}\text{Ti}_{0.05})\text{O}_3$ ceramics with a large energy-density for dielectric energy storage, *RSC Adv.*, 2017, 7:43327- 43333.
- [9] N. H. Fletcher, A. D. Hilton and B. W. Ricketts, Optimization of energy storage density in ceramic capacitors, *J. Phys. D: Appl. Phys.*, 1996, 29:253-258.
- [10] P. Gao, Z. Liu, N. Zhang, H. Wu, A.A. Bokov, W. Ren, Z.G. Ye, New antiferroelectric perovskite system with ultrahigh energy-storage performance at low electric field, *Chem. Mater.*, 2019, 31:979–990.
- [11] X.K. Wei, C.L. Jia, H.C. Du, K. Roleder, J. Mayer, R.E. Dunin-Borkowski, An unconventional transient phase with cycloidal order of polarization in energy-storage antiferroelectric PbZrO_3 , *Adv. Mater.*, 2020, 32(9):1907208
- [12] J. Li, F. Li, Z. Xu, S. Zhang, Multilayer lead-free ceramic capacitors with ultrahigh energy density and efficiency, *Adv. Mater.*, 2018, 30(32):1802155
- [13] N. Liu, R. Liang, Z. Zhou, X. Dong, Designing lead-free bismuth ferrite-based ceramics learning from relaxor ferroelectric behavior for simultaneous high energy density and efficiency under low electric field, *J. Mater. Chem. C*, 2018, 6:10211-10217.
- [14] P. Zhao, H. Wang, L. Wu, L. Chen, Z. Cai, L. Li, X. Wang, High-performance relaxor ferroelectric materials for energy storage applications, *Adv. Energy Mater.*, 2019, 9:1803048
- [15] L.F. Zhu, X.W. Lei, L. Zhao, M.I. Hussain, G.Z. Zhao, B.P. Zhang, Phase structure and energy storage performance for BiFeO_3 - BaTiO_3 based lead-free ferroelectric ceramics, *Ceram. Int.*, 2019, 45:20266–20275

- [16] B. Luo, X. Wang, E. Tian, H. Song, H. Wang, L. Li, Enhanced energy-storage density and high efficiency of lead-free $\text{CaTiO}_3\cdot\text{BiScO}_3$ linear dielectric ceramics, *ACS Appl. Mater. Interfaces*, 2017, 9:19963–19972.
- [17] S.I. Shkuratov, J. Baird, V.G. Antipov, S.Zhang, J.B. Chase, Multilayer PZT 95/5 antiferroelectric film energy storage devices with giant power density, *Adv. Mater.*, 2019, 31:1904819.
- [18] L. Chen, N. Sun, Y. Li, Q. Zhang, L. Zhang, X. Hao, Multifunctional antiferroelectric MLCC with high-energy-storage properties and large field-induced strain, *J. Am. Ceram. Soc.*, 2018, 101:2313–2320.
- [19] Q. Zhang, Y. Dan, J. Chen, Y. Lu, T. Yang, X. Yao, Y. He, Effects of composition and temperature on energy storage properties of $(\text{Pb,La})(\text{Zr,Sn,Ti})\text{O}_3$ antiferroelectric ceramics, *Ceram. Int.*, 2017, 43:11428–11432
- [20] H. Pan, J. Ma, J. Ma, Q. Zhang, X. Liu, B. Guan, L. Gu, X. Zhang, Y.J. Zhang, L. Li, Y. Shen, Y.H. Lin, C.W. Nan, Giant energy density and high efficiency achieved in bismuth ferrite-based film capacitors via domain engineering, *Nat Commun.*, 2018, 9:1813.
- [21] J. Li, Z. Shen, X. Chen, S. Yang, W. Zhou, M. Wang, L. Wang, Q. Kou, Y. Liu, Q. Li, Z. Xu, Y. Chang, S. Zhang, F. Li, Grain-orientation-engineered multilayer ceramic capacitors for energy storage applications, *Nature Materials*, 2020, 19:999–1005.
- [22] H. Pan, F. Li, Y. Liu, Q. Zhang, M. Wang, S. Lan, Y. Zheng, J. Ma, L. Gu, Y. Shen, P. Yu, S. Zhang, L.Q. Chen, Y.H. Lin, C.W. Nan, Ultrahigh–energy density lead-free dielectric films via polymorphic nanodomain design, *Science*, 2019, 365:578–582.
- [23] H. Qi, R. Zuo, A. Xie, A. Tian, J. Fu, Y. Zhang, S. Zhang, Ultrahigh energy-storage density in nanbo_3 -based lead-free relaxor antiferroelectric ceramics with nanoscale domains, *Adv. Funct. Mater.* 2019, 29:1903877.
- [24] R.H. Dungan, R.D. Golding, Metastable ferroelectric sodium niobate, *J. Am. Ceram. Soc.*, 1964, 47(2):73-76.

- [25] A.V. Ulinzheyev, O.E. Fesenko, V.G. Smotrakov, Super-high field-induced phase transitions in NaNbO_3 crystals, *Ferroelectrics Lett.*, 1990, 12(1):17-21.
- [26] A.V. Ulinzheev, A.V. Leiderman, V.G. Smotrakov, V.Y. Topolov, O.E. Fesenko, Phase transitions induced in NaNbO_3 crystals by varying the direction of an external electric field, *Phys. Solid State.*, 1997, 39(6):972-974.
- [27] V.A. Shuvaeva, M.Y. Antipin, R.S.V. Lindeman, O.E. Fesenko, V.G. Smotrakov, Y.T. Struchkov, Crystal structure of the electric-field induced ferroelectric phase of NaNbO_3 , *Ferroelectrics*, 1993, 141(1):307-331.
- [28] T. Arioka, H. Taniguchi, M. Itoh, K. Oka, R. Wang, D. Fu, Ferroelectricity in NaNbO_3 : Revisited, *Ferroelectrics*, 2010, 401(1):51-55.
- [29] H. Shimizu, K. Kobayashi, Y. Mizuno and C. A. Randall, Advantages of low partial pressure of oxygen processing of alkali niobate: NaNbO_3 , *J. Am. Ceram. Soc.*, 2014, 97(6):1791-1796.
- [30] Y. Xu, W. Hong, Y. Feng, X. Tan, Antiferroelectricity induced by electric field in NaNbO_3 -based lead-free ceramics, *Appl. Phys. Lett.*, 2014, 104(5):052903.
- [31] D. Fu, T. Arioka, H. Taniguchi, T. Taniyama, M. Itoh, Ferroelectricity and electromechanical coupling in $(1-x)\text{AgNbO}_3$ - $x\text{NaNbO}_3$ solid solutions, *Appl. Phys. Lett.*, 2011, 99:012904.
- [32] H. Shimizu, H. Guo, S.E. Reyes-Lillo, Y. Mizuno, K.M. Rabec, C.A. Randall, Lead-free antiferroelectric: $x\text{CaZrO}_3$ - $(1-x)\text{NaNbO}_3$ system ($0 \leq x \leq 0.10$), *Dalton Trans.*, 2015, 44:10763–10772.
- [33] Z. Liu, J. Lu, Y. Mao, P. Ren, H. Fan, Energy storage properties of NaNbO_3 - CaZrO_3 ceramics with coexistence of ferroelectric and antiferroelectric phases, *J. Eur. Ceram. Soc.*, 2018, 38(15):4939-4945.
- [34] H. Qi, R. Zuo, A. Xie, J. Fu, D. Zhang, Excellent energy-storage properties of NaNbO_3 -based lead-free antiferroelectric orthorhombic P-phase (Pbma) ceramics with repeatable double polarization-field loops, *J. Eur. Ceram. Soc.*, 2019, 39:3703–3709.
- [35] C. Kittel, Theory of antiferroelectric crystals, *Phys. Rev.*, 1951, 82, 729.

- [36] A. Chauhan, S. Patel, R. Vaish, C.R. Bowen, Anti-ferroelectric ceramics for high energy density capacitors, *Materials*, 2015, 8:8009-8031.
- [37] W. Huang, Y. Chen, X. Li, G. Wang, N. Liu, S. Li, M. Zhou, X. Dong, Ultrahigh recoverable energy storage density and efficiency in barium strontium titanate-based lead-free relaxor ferroelectric ceramics, *Appl. Phys. Lett.*, 2018, 113:203902.
- [38] F. Li, K.W. Kwok, Fabrication of transparent electro-optic $(K_{0.5}Na_{0.5})_{1-x}Li_xNb_{1-x}Bi_xO_3$ lead-free ceramics, *J. Eur. Ceram. Soc.*, 2013, 33:123–130.
- [39] H. Yang, F. Yan, Y. Lin, T. Wang, Novel strontium titanate-based lead-free ceramics for high-energy storage applications, *ACS Sustain. Chem. Eng.*, 2017, 5:10215–10222.
- [40] Z. Yang, H. Du, L. Jin, Q. Hu, S. Qu, Z. Yang, Y. Yu, X. Wei, Z. Xu, A new family of sodium niobate-based dielectrics for electrical energy storage applications, *J. Eur. Ceram. Soc.*, 2019, 39:2899–2907.
- [41] K. Uchino, S. Nomura, Critical exponents of the dielectric constants in diffused-phase-transition crystals, *Ferroelectrics*, 2011, 44:55–61.
- [42] L. Yang, X. Kong, F. Li, H. Hao, Z. Cheng, H. Liu, J.F. Li, S. Zhang, Perovskite lead-free dielectrics for energy storage applications, *Progress in Materials Science*, 2019, 102:72–108.
- [43] N.J. Lóh, L. Simão, C.A. Faller, A. De Noni Jr, O.R.K. Montedo, A review of two-step sintering for ceramics, *Ceram. Int.*, 2016, 42(11):12556-12572.
- [44] A. Xie, H. Qi, R. Zuo, Achieving Remarkable Amplification of energy-storage density in two-step sintered $NaNbO_3$ – $SrTiO_3$ antiferroelectric capacitors through dual adjustment of local heterogeneity and grain scale, *ACS Appl. Mater. Interfaces* 2020, 12:19467–19475.